Computer Physics Communications 295 (2024) 109020

Contents lists available at ScienceDirect

Computer Physics Communications

journal homepage: www.elsevier.com/locate/cpc

Computational Physics

Energy and charge conserving semi-implicit particle-in-cell model for simulations of high-pressure plasmas in magnetic traps ☆,☆☆

E.A. Berendeev [a,b], I.V. Timofeev [a,b,*], V.A. Kurshakov [a,b]

[a] Novosibirsk State University, Pirogov st., 1, Novosibirsk, 630090, Russian Federation
[b] Budker Institute of Nuclear Physics SB RAS, Lavrent'ev av., 11, Novosibirsk, 630090, Russian Federation

ARTICLE INFO

Keywords:
Particle-in-cell simulations
Mirror traps
High-β plasma

ABSTRACT

The paper presents a new particle-in-cell model for fully kinetic simulations of plasma confinement regimes with high relative pressure. These regimes are considered as the most promising ones for fusion reactor proposals based on field reversed configurations, mirror and multi-cusp magnetic traps. Formation of an equilibrium high-pressure plasma with a fully excluded or reversed magnetic field cannot be investigated using the simplified magnetohydrodynamic and gyrokinetic approaches. A correct description of the electron dynamics under close proximity of zero and strong magnetic field regions can only be achieved within the framework of the kinetic theory that can be implemented most efficiently by the particle-in-cell method. The full-scale particle-in-cell simulations of modern fusion experiments require the use of finite-difference schemes in which temporal steps exceed the period of fastest electron oscillations at the plasma or even cyclotron frequencies and spatial steps do not have to resolve the Debye radius. This requirement is satisfied by implicit schemes capable of conserving the total energy of the system. The particle-in-cell model presented in this paper is based on the energy conserving semi-implicit approach as a predictive step and a new method for suppressing the electrostatic noise inherent in it as a corrective step. This two-step algorithm provides not only accurate energy conservation, but also the exact local fulfillment of the Gauss law.

1. Introduction

As is known, the most promising way to rise the energy confinement time in magnetic traps with open field lines is to increase the relative plasma pressure β. The maximum value of this parameter $\beta = 1$ is reached when the plasma completely expels the magnetic field and is kept in equilibrium by the pressure of this field at the periphery. Modern proposals to build a fusion reactor using mirror [1–3], multi-cusp [4,5] and field reversed (FRC) [6–8] magnetic configurations are based on the transit to these high-β regimes. To simulate them, it is necessary to create a numerical model that would correctly describe the main physical processes either facilitating or hindering the establishment of a high-β equilibrium configuration in the proposed fusion schemes. In this paper, proposing such a model, we will focus on the special set of parameters that is realized in laboratory experiments at the CAT (Compact Axisymmetric Toroid) facility [10] at the Budker Institute of Nuclear Physics SB RAS. In these experiments, high-beta plasma equilibria such as diamagnetic bubble [1] or FRC are planned to be created using high-power neutral injection [9].

The main challenge in numerical simulation of fusion plasma devices is a huge dynamic range between the micro- and macroscales of the processes of interest. The most detailed kinetic description of plasma provided by Particle-In-Cell (PIC) models requires to resolve the Larmor rotation of electrons or their fast oscillations at the plasma frequency throughout the whole duration of the experiment. In addition, the numerical scheme stability ties the spatial grid step Δx to the plasma Debye radius, and in electromagnetic codes to the path $c\Delta t$ traveled by the light in a time step (the Courant-Friedrichs-Lewy (CFL) condition). For example, in the CAT experiment, the duration of neutral injection will be several milliseconds, which is 8 orders of magnitude

☆ The work is supported by Russian Science Foundation (grant N0 21-72-10071).
☆☆ The review of this paper was arranged by Prof. David W. Walker.
* Corresponding author at: Novosibirsk State University, Pirogov st., 1, Novosibirsk, 630090, Russian Federation.
E-mail address: I.V.Timofeev@inp.nsk.su (I.V. Timofeev).

https://doi.org/10.1016/j.cpc.2023.109020
Received 8 May 2023; Received in revised form 30 October 2023; Accepted 15 November 2023
Available online 20 November 2023

longer than the period of electron cyclotron rotation in an unperturbed magnetic field. Moreover, the Debye radius of the starting plasma turns out to be 4–5 orders of magnitude smaller than the linear dimensions of the experimental setup. In the simplest implementation of the PIC method, based on explicit finite difference schemes [11,12], the particle coordinates and momenta at a new time step are calculated using the values of electromagnetic (EM) fields from the previous step. The main disadvantage of these schemes is the lack of exact energy conservation, that imposes the above severe restrictions on the size of the space and time steps (CFL condition) and limits the modeling of long-term ion dynamics due to the accumulation of an error in the total energy.

In this regard, the most popular way to model the fusion plasmas is to use the simplified hybrid approaches when ions are still described by the PIC method but electrons are simulated using either the magnetohydrodynamics [13,14], or gyrokinetics [15]. Such approaches, however, are incapable of describing the regions with weak or zero magnetic fields, which must inevitably appear in the FRC or diamagnetic bubble. Thus, the only way to correctly model the plasma in configurations with high β is to preserve the kinetic description for both ions and electrons. This can be implemented in the PIC model only by using implicit finite difference schemes. Indeed, if the coordinates and velocities of particles are updated according to the values of EM fields not only from the past, but also from the future, it becomes possible to accurately conserve the total energy of the system. As a result, the numerical scheme remains stable even at large time steps that do not resolve the plasma and cyclotron frequencies of electrons. The capability of a time step to exceed the electron cyclotron period in highly magnetized regions even by a few times makes the problem of a full-scale description of the CAT experiment realistic.

In recent years, many implicit schemes for integrating the system of Vlasov-Maxwell equations have been proposed. They can be divided into two groups: fully implicit [16,17] and semi-implicit schemes [18–23]. In the former case, the equations of motion for particles and the Maxwell equations for fields are solved simultaneously using nonlinear Newton-Krylov iterations, and the energy of the system can be conserved with any predetermined accuracy. In the semi-implicit approach, the computational cycle is constructed in the same way as in explicit PIC schemes, and the response of particles to the field in the future is taken into account in Maxwell's equations through the linear current. While in the Direct Implicit Method (DIM) [18,19] and the Implicit Moment Method (IMM) [20–22] the particles response is only approximately linear leading to nonconservation of energy, in the Energy Conserving Semi-Implicit Method (ECSIM) [23] the linearity of the current is not the result of any approximations, which allows energy to be conserved at discrete time steps exactly. It is worth noting that the ability to accurately conserve energy is very important for modeling collisional effects in plasma, since it allows this conservation law to be preserved when PIC algorithms work together with the Monte Carlo algorithm of Coulomb collisions [24]. Obviously, semi-implicit schemes turn out to be several times more efficient from a computational point of view than fully implicit ones because of the absence of nonlinear iterations.

To simulate plasma confinement in mirror traps, the charge conservation law is also important. Failure to comply with the finite-difference analog of the Gauss law can lead to an increased level of small-scale electrostatic fluctuations. This noise may affect the losses of particles and energy from the trap. It is known that in PIC models the evolution of EM fields is calculated only on the basis of Maxwell's rotary equations, while in order to fulfill the divergent equations at each time step ($\operatorname{div}\mathbf{E} = 4\pi\rho$ and $\operatorname{div}\mathbf{B} = 0$) it is necessary that the current and charge densities satisfy the continuity equations. The second of these equations is automatically satisfied if the spatial discretization provides the vector equality $\operatorname{div}(\operatorname{rot}\mathbf{A}) = 0$, while the fulfillment of the first equation depends on how the current is calculated. In PIC codes, this problem is solved either by correcting the potential part of the electric field by solving the Poisson equation according to the actual charge density distribution on the grid, or by using the density decomposition method [25] and calculating the electric current components directly from the continuity equation. For simultaneous charge and energy conservation in the ECSIM, recent works have proposed to either correct the positions of particles at the end of the computational cycle in order to fulfill the Gauss law [26], or, based on a two-stage predictor-corrector scheme [27], first predict the fields from the ECSIM linear current, which does not save charge, and then correct the fields from the new current that satisfies the continuity equation. It is interesting that, in the framework of the finite element method used in [27], the correct current has the similar form as in the ECSIM method, with the only difference that the trajectory-averaged value $\left\langle W(\mathbf{x}_p(t) - \mathbf{x}_g)\right\rangle$ for each macroparticle is used instead of its instantaneous shape at the half step $W(\mathbf{x}_p^{n+1/2} - \mathbf{x}_g)$. Unfortunately, it remains unclear how much the neglect of the curl part of the current correction in this model affects the level of electromagnetic fluctuations and how to correct particle velocities when currents are created by several particle species.

In this paper, to simulate high-β regimes in fusion facilities, we propose to reformulate the predictor-corrector scheme of [27] for the standard spatial discretization on the Yee grid modifying substantially the corrective step. In the proposed scheme, the prediction of unknown quantities at a new time step is based on the energy-saving ECSIM [23] method, and the charge conservation is ensured by the transition to the current calculated using the Density Decomposition Method of Esirkepov [25] at the corrective step. In contrast to the work of [27], not only the electric, but also the magnetic field is subjected to correction here. In this case, the energy conservation law requires that the correction of the kinetic energy should compensate the change in work done by the electric field on the particle currents. Since the correct current in the Esirkepov's method is calculated separately for each particle, there is a natural opportunity not only to make a local correction of velocities (with its own coefficient for each cell, taking into account only those fields that actually act on the particle), but also to separate the contributions to this work from different particle species. The latter circumstance is important for describing experiments in magnetic traps, when the current is generated by both electrons and a population of high-energy ions.

2. Description of the model

Our goal is to propose an implicit PIC model that would allow the use of large steps ($\Delta t > \omega_p^{-1}, \Omega_e^{-1}$) and would be suitable for full-scale simulations of laboratory experiments, which is possible when the key laws of energy and charge conservation are fulfilled. Further, we will construct a PIC algorithm for advancing particles and fields to a new time step based on the similar predictor-corrector scheme that was proposed in [27]. First, we predict the unknown values of the coordinates $\mathbf{x}_p^{n+1}$ and the velocities $\tilde{\mathbf{v}}_p^{n+1}$ of the particles, as well as the values of the EM fields $\tilde{\mathbf{E}}_g^{n+1}$ and $\tilde{\mathbf{B}}_g^{n+1}$ on the grid at the new step $t_{n+1} = (n+1)\Delta t$ using the semi-implicit ECSIM method [23] that conserves energy but does not conserve charge. Then, at the corrective step, the current $\tilde{\mathbf{J}}_p^{n+1}$, which does not satisfy the continuity equation, is replaced by the current $\mathbf{J}_p^{n+1}$ calculated using the Esirkepov decomposition method [25]. After that, we correct the fields $\tilde{\mathbf{E}}_p^{n+1}, \tilde{\mathbf{B}}_p^{n+1} \to \mathbf{E}_p^{n+1}, \mathbf{B}_p^{n+1}$ and perform local renormalization of particle velocities $\tilde{\mathbf{v}}_p^{n+1} \to \mathbf{v}_p^{n+1}$ in order to restore the energy conservation.

At the prediction stage, to move particles, we will use the following finite-difference scheme:

$$\mathbf{x}_p^{n+1/2} = \mathbf{x}_p^n + \frac{\Delta t}{2}\mathbf{v}_p^n, \tag{1}$$

$$\tilde{\mathbf{v}}_p^{n+1} = \mathbf{v}_p^n + \frac{q_p \Delta t}{m_p}\left(\tilde{\mathbf{E}}_p^{n+1/2} + \left[\tilde{\mathbf{v}}_p^{n+1/2} \times \mathbf{B}_p^n\right]\right), \tag{2}$$

where the half-step speed $\tilde{\mathbf{v}}_p^{n+1/2} = (\mathbf{v}_p^n + \tilde{\mathbf{v}}_p^{n+1})/2$ is half the sum of the values at the old and new steps, and the EM fields acting on a finite size

macroparticle with the form-factor W are determined by interpolation of their grid values

$$\tilde{\mathbf{E}}_p^{n+1/2}(\mathbf{x}_p^{n+1/2}) = \sum_g \left(\frac{\mathbf{E}_g^n + \tilde{\mathbf{E}}_g^{n+1}}{2} \right) W(\mathbf{x}_p^{n+1/2} - \mathbf{x}_g), \tag{3}$$

$$\mathbf{B}_p^n(\mathbf{x}_p^{n+1/2}) = \sum_g \mathbf{B}_g^n W(\mathbf{x}_p^{n+1/2} - \mathbf{x}_g). \tag{4}$$

Here and below, time is measured in units of the reciprocal plasma frequency of electrons ($\omega_p = \sqrt{4\pi e^2 n_0/m_e}$), particle velocities and coordinates — in the speed of light c and the length of the plasma skin-depth c/ω_p, charge q_p and mass m_p of particles — in units of charge e and mass m_e of electron, fields are measured in units of $m_e c\omega_p/e$, and particles density and current — in units of n_0 and $en_0 c$. To solve Maxwell's equations in finite-difference form

$$\tilde{\mathbf{B}}_g^{n+1} = \mathbf{B}_g^n - \Delta t \left(\mathrm{rot}\, \tilde{\mathbf{E}}^{n+1/2}\right)_g, \tag{5}$$

$$\tilde{\mathbf{E}}_g^{n+1} = \mathbf{E}_g^n - \Delta t \tilde{\mathbf{J}}_g^{n+1/2} + \Delta t \left(\mathrm{rot}\, \tilde{\mathbf{B}}^{n+1/2}\right)_g, \tag{6}$$

where $\tilde{\mathbf{B}}_g^{n+1/2} = (\mathbf{B}_g^n + \tilde{\mathbf{B}}_g^{n+1})/2$, it is necessary to calculate the density of the electric current created by computational particles at a half step:

$$\tilde{\mathbf{J}}_g^{n+1/2} = \sum_p q_p \tilde{\mathbf{v}}_p^{n+1/2} W(\mathbf{x}_p^{n+1/2} - \mathbf{x}_g). \tag{7}$$

Using Eq. (2), the intermediate velocity $\tilde{\mathbf{v}}_p^{n+1/2}$ is expressed in terms of the electric field $\tilde{\mathbf{E}}_p^{n+1/2}$, which makes it possible to establish a linear relationship between the grid values of the current and the electric field in the future:

$$\tilde{\mathbf{J}}_g^{n+1/2} = \mathbf{I}_g + \frac{\Delta t}{4} \sum_{g'} \hat{\mathbf{L}}_{gg'} (\mathbf{E}_{g'}^n + \tilde{\mathbf{E}}_{g'}^{n+1}), \tag{8}$$

$$\mathbf{I}_g = \sum_p \frac{q_p}{1+\alpha_p^2} \left[\mathbf{v}_p^n + \alpha_p \left[\mathbf{v}_p^n \times \mathbf{h} \right] + \alpha_p^2 \mathbf{h} (\mathbf{h}\mathbf{v}_p^n) \right] W(\mathbf{x}_p^{n+1/2} - \mathbf{x}_g), \tag{9}$$

$$\hat{\mathbf{L}}_{gg'} = L_{gg'}^{ij} = \sum_p \frac{q_p^2}{m_p(1+\alpha_p^2)} \left[\delta_{ij} + \alpha_p e_{ijm} h_m + \alpha_p^2 h_i h_j \right] \times W(\mathbf{x}_p^{n+1/2} - \mathbf{x}_g) W(\mathbf{x}_p^{n+1/2} - \mathbf{x}_{g'}), \tag{10}$$

$$\alpha_p = \frac{q_p \Delta t}{2 m_p} |\mathbf{B}_p^n|, \qquad \mathbf{h} = \frac{\mathbf{B}_p^n}{|\mathbf{B}_p^n|}. \tag{11}$$

Here, δ_{ij} and e_{ijm} are understood as the unit and absolutely antisymmetric tensors (in a three-dimensional Cartesian space, the indices i and j range over the values x, y, z, and g and g' run through all nodes of the spatial grid). It should be noted that, unlike other semi-implicit schemes [19,21,22], the linear response of particles to EM fields in the ECSIM method is not a result of any approximations. Substituting the current (8) into the Maxwell's equations and also excluding the magnetic field from them, we obtain a system of linear algebraic equations for grid electric fields $\tilde{E}_g^{n+1}$ at a new step. Having this system solved, we then calculate the preliminary velocities for all particles $\tilde{\mathbf{v}}_p^{n+1}$. Completing the computational cycle, we determine the particle positions at the $n+1$ step:

$$\mathbf{x}_p^{n+1} = \mathbf{x}_p^{n+1/2} + \frac{\Delta t}{2} \tilde{\mathbf{v}}_p^{n+1}. \tag{12}$$

Representing the current in the form (7) is convenient for ensuring the exact conservation of energy, but if we calculate the rate of change in the charge density from the new particle positions, it turns out that this value does not satisfy the continuity equation with this current. This means that the Gauss law is not satisfied in such a scheme, and parasitic fluctuations of the electric field can grow in the system. The current that conserves the charge must satisfy the finite-difference continuity equation

$$\Delta\rho_g = \sum_p q_p \left[W(\mathbf{x}_p^{n+1} - \mathbf{x}_g) - W(\mathbf{x}_p^n - \mathbf{x}_g) \right] = -\Delta t \left(\mathrm{div}\, \mathbf{J}^{n+1/2}\right)_g. \tag{13}$$

However, if the new value of the current $\mathbf{J}_g^{n+1/2}$ is calculated by the Esirkepov's method [25] directly from Eq. (13) with the same particle shape W as at the prediction step, we will face the following difficulty. The fact is that the Esirkepov current from each particle makes a non-zero contribution to a smaller number of nodes than the current (7) predicted from the particle shape in the middle of its trajectory. As will be shown in Sec. 3.3, a large local difference in the current density leads to the need for a strong local field corrections and excites a numerical instability when trying to introduce these corrections into the particle energy. The problem is solved if a smoother particle kernel $\tilde{W}$ is used at the correction stage. For example, the numerical scheme remains stable if the Esirkepov current is calculated using the parabolic kernel instead of the linear one. In addition, since the particle trajectory at each time step consists of two straight-line segments, in order to improve accuracy, the calculation of the Esirkepov current consists of two stages corresponding to each of these segments:

$$\Delta\rho_g = \sum_p q_p \left[\tilde{W}(\mathbf{x}_p^{n+1} - \mathbf{x}_g) - \tilde{W}(\mathbf{x}_p^{n+1/2} - \mathbf{x}_g) \right] + \sum_p q_p \left[\tilde{W}(\mathbf{x}_p^{n+1/2} - \mathbf{x}_g) - \tilde{W}(\mathbf{x}_p^n - \mathbf{x}_g) \right]. \tag{14}$$

Then, solving the Maxwell equations with a new source current, we obtain the corrected spatial distribution of EM fields $\mathbf{E}_g^{n+1}$ and $\mathbf{B}_g^{n+1}$. The quantity preserved by the Maxwell's equations

$$\sum_g \left[\frac{1}{2} \left(|\mathbf{E}_g^{n+1}|^2 - |\mathbf{E}_g^n|^2 + |\mathbf{B}_g^{n+1}|^2 - |\mathbf{B}_g^n|^2 \right) + \Delta t \mathbf{J}_g^{n+1/2} \mathbf{E}_g^{n+1/2} + \Delta t \nabla_g \cdot \left[\mathbf{E}_g^{n+1/2} \times \mathbf{B}_g^{n+1/2} \right] \right] = 0 \tag{15}$$

has the meaning of the energy conservation law if the work of the corrected electric field on the new current is equal to the change in the kinetic energy of the particles:

$$\sum_g \Delta t \mathbf{J}_g^{n+1/2} \mathbf{E}_g^{n+1/2} = \sum_p \frac{m_p}{2} \left(|\mathbf{v}_p^{n+1}|^2 - |\mathbf{v}_p^n|^2 \right). \tag{16}$$

Since the same equality holds at the prediction stage, the correction for particle velocities must be determined by the change in work:

$$\sum_p \frac{m_p}{2} \left(|\mathbf{v}_p^{n+1}|^2 - |\tilde{\mathbf{v}}_p^{n+1}|^2 \right) = \Delta t \sum_g \left[\mathbf{J}_g^{n+1/2} \mathbf{E}_g^{n+1/2} - \tilde{\mathbf{J}}_g^{n+1/2} \tilde{\mathbf{E}}_g^{n+1/2} \right]. \tag{17}$$

The simplest way to restore the energy conservation law at the corrective step is to globally correct the particle velocities $\mathbf{v}_p^{n+1} = \lambda \tilde{\mathbf{v}}_p^{n+1}$ with the single coefficient

$$\lambda^2 = 1 + \frac{\Delta t \sum_g \left[\mathbf{J}_g^{n+1/2} \mathbf{E}_g^{n+1/2} - \tilde{\mathbf{J}}_g^{n+1/2} \tilde{\mathbf{E}}_g^{n+1/2} \right]}{\sum_p m_p |\tilde{\mathbf{v}}_p^{n+1}|^2/2}. \tag{18}$$

However, due to the fact that the current in the Esirkepov method is calculated as the sum of the contributions of individual particles $\mathbf{J}_g^{n+1/2} = \sum_p \mathbf{J}_g^p$, the energy correction can be carried out locally in accordance with the work done on the particles in the given cell C:

$$\sum_{p\in C} \frac{m_p}{2} \left(|\mathbf{v}_p^{n+1}|^2 - |\tilde{\mathbf{v}}_p^{n+1}|^2 \right) = \Delta t \sum_{p\in C} \left[\sum_{g\in p} \mathbf{J}_g^p \mathbf{E}_g^{n+1/2} - q_p \tilde{\mathbf{v}}_p^{n+1/2} \tilde{\mathbf{E}}_p^{n+1/2} \right], \tag{19}$$

where the summation is over the particles from the given cell and over those grid nodes where the particle p creates a nonzero current. Introducing a local correction factor for each cell

$$\lambda_C^2 = 1 + \frac{\Delta t \sum\limits_{p\in C}\left[\sum\limits_{g\in p}\mathbf{J}_g^p\mathbf{E}_g^{n+1/2} - q_p\tilde{\mathbf{v}}_p^{n+1/2}\tilde{\mathbf{E}}_p^{n+1/2}\right]}{\sum\limits_{p\in C} m_p|\tilde{\mathbf{v}}_p^{n+1}|^2/2}, \tag{20}$$

the new particle velocity can be calculated as $\mathbf{v}_p^{n+1} = \lambda_C\tilde{\mathbf{v}}_p^{n+1}$. By dividing the currents into components from different types of particles, one can introduce individual correction factors for each type.

3. Testing the model

3.1. Gyrokinetic drifts in stationary fields

Since in equilibrium plasma configurations with high β a transition layer should be formed between the regions of weak and strong magnetic fields with a width of the order of the ion Larmor radius $\sim\rho_i$ in the vacuum field [28], the grid step should resolve inhomogeneities on the scale of ρ_i, but can exceed the radius of electron cyclotron rotation ρ_e. In the CAT experiment, the typical velocities of 15 keV ions and thermal electrons are comparable with each other ($v_i/c = 0.0056$ and $v_e/c = 0.01 - 0.02$), but their Larmor radii in the maximum magnetic field $\Omega_e/\omega_p = 0.4$ are significantly different ($\rho_i = 25\,c/\omega_p$ and $\rho_e = (0.025-0.05)\,c/\omega_p$). The admissible spatial resolution $\Delta x \sim c/\omega_p$ makes it possible to use relatively large time steps $\Delta t = \Delta x/(2v_e) \sim 25\,\omega_p^{-1}$ allowing the particle to pass distance equal to half of the grid spacing. In the magnetic field of the CAT facility ($\Omega_e/\omega_p = 0.2 - 0.4$) at the plasma density of $n_0 = 10^{13}$ cm^{-3}, such a time step is sufficient to resolve oscillations with the ion cyclotron frequency Ω_i, but it turns out to be too large to resolve the cyclotron rotation of electrons ($\Delta t = (5-10)/\Omega_e$). However, as long as the scale of spatial inhomogeneities in highly magnetized regions of the plasma significantly exceeds the size of the electron gyro-orbit, one can neglect the deviations of particles from the trajectories of their Larmor centers and reproduce their dynamics with the same accuracy as in the drift approximation. Even taking into account that the explicit Boris algorithm used in our model overestimates the effective Larmor radius for large time steps $\rho_{\text{eff}} = \rho_e\sqrt{1+\Omega_e^2\Delta t^2/4}$ [29,30], the drift approximation remains applicable up to the values of interest to us

$$\Omega_e\Delta t = 5 - 10 \ll \frac{B}{|\nabla B|\rho_e} \sim \frac{\rho_i}{\rho_e}. \tag{21}$$

Let us make sure that the Boris pusher correctly reproduces the main drifts of an individual electron in stationary electromagnetic fields even at large time steps $1 < \Omega_e\Delta t < B/(\rho_e|\nabla B|)$. In the uniform magnetic field $B_z = 0.2$, the electron starting from the point $\mathbf{x}_e = (0,-0.1,0)$ with the velocity $\mathbf{v}_e = (0.02,0,0)$ should move in a circle with the radius $\rho_e = v_e/B_z = 0.1$. Fig. 1 shows that the electron stays on this circular trajectory even when its Larmor frequency is not well resolved.

If a uniform electric field $E_y = 0.001$ is also applied to a given magnetic field, then the electron will begin to experience the $\mathbf{E}\times\mathbf{B}$-drift, moving (on average) in the x direction with a velocity of $V_E = E_y/B_z = 0.005$. Fig. 2a shows that the electron trajectory at large steps, although it ceases to look like a spiral, still continues to lie in the same strip that is swept out on the (x,y) plane by the real trajectory. From Fig. 2b one can also see that the x-coordinate of a particle follows, on average, the law of motion of its Larmor center $V_E t$, advancing or lagging behind in different phases of rotation by less than ρ_e.

A similar behavior is also observed in the inhomogeneous magnetic field $B_z(y) = 0.2(1-0.8y)$. In this case, the drift along x is caused by the transverse component of the force $\mathbf{F} = -\mu\nabla B$ (where $\mu = m_e v_\perp^2/(2B)$ is the magnetic moment of the Larmor circle), which causes the Larmor center to move in the direction of $\mathbf{F}\times\mathbf{B}$ with the velocity

$$V_{\nabla B} = \frac{v_\perp^2}{2B_z^2(0)}\frac{\partial B_z}{\partial y}.$$

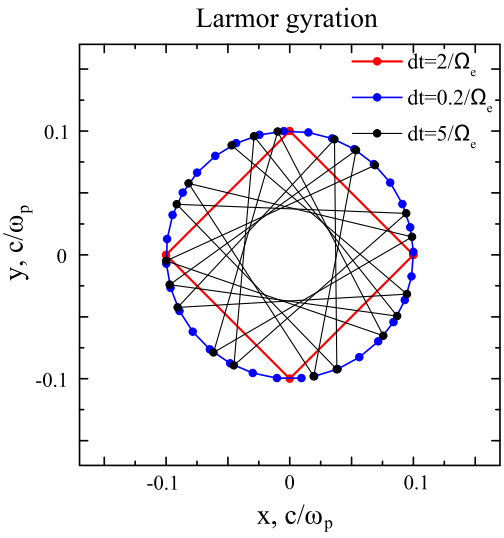

Fig. 1. Larmor rotation of an electron in the uniform magnetic field $B_z = 0.2$ for different time steps Δt.

It can be seen from Fig. 3 that, up to deviations by the Larmor radius, the electron drift trajectory is well reproduced in the model even at large time steps.

Thus, in weakly magnetized regions of plasma, the proposed PIC model can provide an accurate kinetic description of both ions and electrons, and in the strong magnetic field, the same model, while remaining kinetic for ions, is able to reproduce the electron dynamics in the drift approximation.

3.2. Confinement of test particles in a compact cell of the CAT

The main goal of the created model is to study the long-term dynamics of plasma during its heating and confinement in mirror traps. In the CAT experiment, a plasma with a characteristic density $n_0 = 10^{13}$ cm^{-3} and a high relative pressure $\beta \approx 1$ is planned to be created in a compact mirror cell consisting of two current coils separated by $L = 344\ c/\omega_p \approx 60$ cm. Neglecting the thickness of coils with radius R, the axisymmetric magnetic field in such a system can be calculated as follows:

$$B_r(r,z) = IR\int_0^{2\pi} d\varphi\cos\varphi\left[\frac{z}{(R^2+z^2+r^2-2Rr\cos\varphi)^{3/2}} + \frac{z-L}{(R^2+(z-L)^2+r^2-2Rr\cos\varphi)^{3/2}}\right], \tag{22}$$

$$B_z(r,z) = IR\int_0^{2\pi} d\varphi(R-r\cos\varphi)\left[\frac{1}{(R^2+z^2+r^2-2Rr\cos\varphi)^{3/2}} + \frac{1}{(R^2+(z-L)^2+r^2-2Rr\cos\varphi)^{3/2}}\right]. \tag{23}$$

To provide the mirror ratio

$$\mathcal{R} = \frac{B_z(0,0)}{B_z(0,L/2)} = 2$$

used in the experiment on the axis of the system, the radius of the coils must be equal to $R = L/2.39$. The current $I = \Omega_{max}R/(8\pi)(1 + L^2/R^2/4)^{3/2}$ (measured in units of ec/r_e) is chosen so that the dimensionless field in the mirror $\Omega_{max} = eB_{max}/(m_e c\omega_p)$ corresponds to its experimental value $B_{max} = 0.4$ T.

The longitudinal component of the force $\mathbf{F} = -\mu\nabla B$ leads to the confinement between the mirrors of those particles that lie outside the loss cone $v_\parallel < v_\perp\sqrt{\mathcal{R}-1}$. Since the drift under the action of the transverse

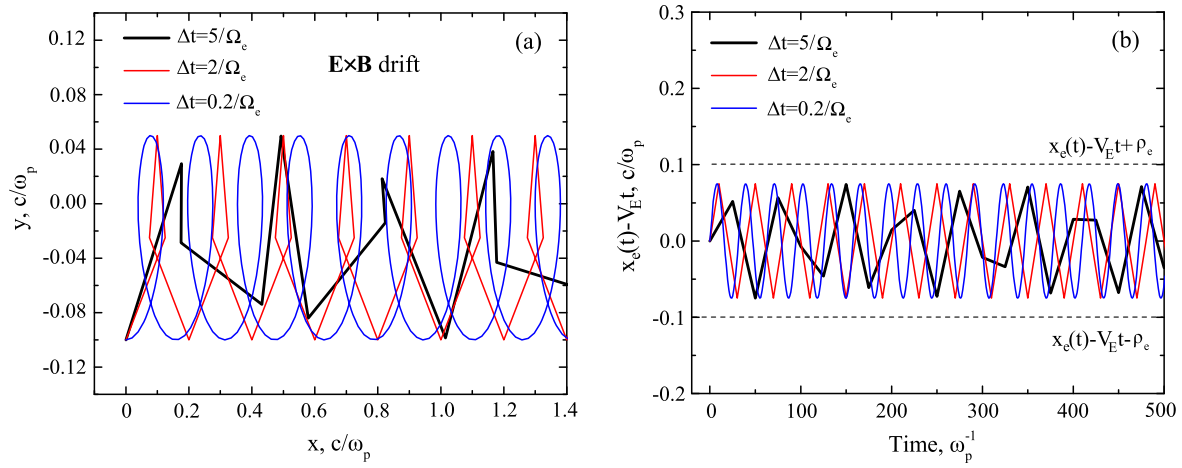

Fig. 2. $\mathbf{E}\times\mathbf{B}$-drift of an electron with $v_\perp = 0.02$ in uniform crossed fields $B_z = 0.2$ and $E_y = 0.001$ at different time steps. (a) Trajectory on the plane (x, y), (b) deviation of the x-coordinate of the particle from the gyrokinetic trajectory of the center of the Larmor circle $V_E t$.

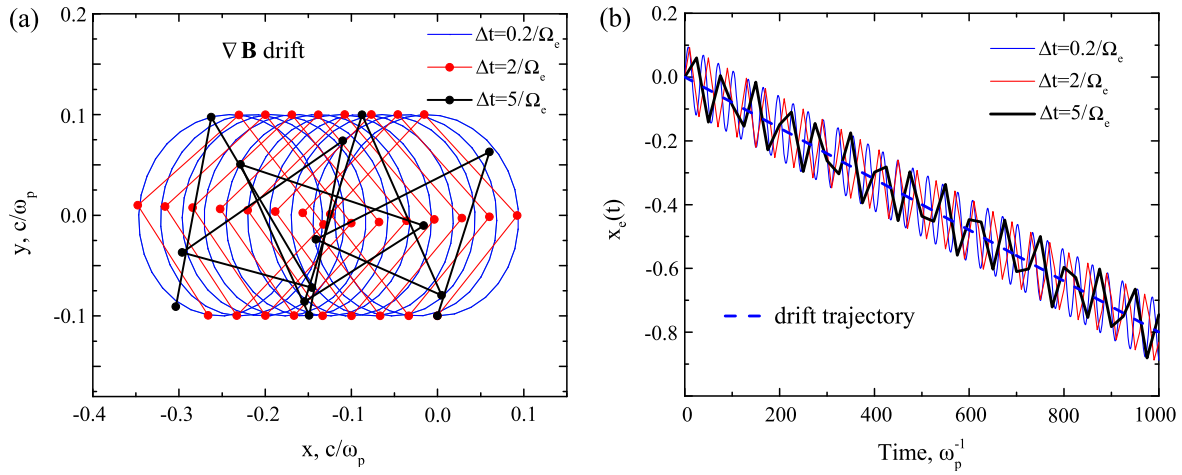

Fig. 3. Drift of an electron with $v_\perp = 0.02$ under the action of ∇B in the inhomogeneous magnetic field $B_z = 0.2(1 - 0.8y)$ at different time steps. (a) Trajectory on the plane (x, y), (b) comparison of the law of particle motion along x with the gyrokinetic trajectory $V_{\nabla B} t$.

component of the same force $\mathbf{F}$ is correctly reproduced by the model, an additional check at what conditions and for how long a particle can be confined between the mirrors seems redundant. However, before modeling the plasma, it needs to make sure that discretization of the external field on a grid with the relatively large step $\Delta x = 1\ c/\omega_p \approx 1.7$ mm as well as interpolation of the grid field values to a finite-size particle does not influence on particle losses over the time of the experiment.

Let us investigate how strongly the finite grid effects influence on the particle trajectories, using the example of an electron and a proton, whose starting coordinates and velocities are equal to $\mathbf{x}_e = (0, 27, L/2)$, $\mathbf{v}_e = (0.02, 0, 0.018)$, $\mathbf{x}_i = (0, 27, L/2)$, $\mathbf{v}_i = (0.003, 0, 0.0025)$. We first calculate the trajectories of point-shape particles $\mathbf{x}_e(t)$ and $\mathbf{x}_i(t)$ in the magnetic field given by the formulas (22) and (23) in continuous space. In Fig. 4a and 4b, these trajectories are shown for the case $\Delta t = 25$. It can be seen that the particles perform bounce oscillations along z between the stopping points located near the mirrors. Due to the small Larmor radius, the electron is actually tied to the magnetic field line, drifting weakly in the azimuthal direction (along x), while the proton trajectory turns out to be more complex and covers the trap axis. Since the field inhomogeneities can be neglected at the electron gyro-radius, the conservation of the magnetic moment $\mu = \text{const}$ is well satisfied for the electron. This means that the magnetic field at its stopping point is determined by the angle of the velocity vector in the central plane of the trap $B_{st}/B_{\min} = 1 + (v_\parallel/v_\perp)^2 \approx 1.81$, and the radius of its magnetic field line varies from the maximum value $y_{\max} = 27$ in the central plane to the minimum value $y_{\min} = y_{\max}\sqrt{B_{\min}/B_{st}} \approx 20.07$ at the stopping point. Solving the equation $B(y_{min}, z) = B_{st}$, one can determine the z-coordinates of the stopping points ($z_{min} = 49.6$, $z_{max} = 294.4$). It can be seen that for the electron the simplification $\mu = \text{const}$ allows to accurately determine the restrictions on the region accessible for its motion.

In the PIC model, a particle with the coordinate $\mathbf{x}_p$ is actually a finite-size cloud of charge with the form-factor $W(\mathbf{x} - \mathbf{x}_p) = W(x - x_p)W(y - y_p)W(z - z_p)$, where

$$W(x - x_p) = \begin{cases} 1 - \left|x - x_p\right|/\Delta x, & \left|x - x_p\right| < \Delta x, \\ 0, & \text{otherwise}, \end{cases} \tag{24}$$

and the magnetic field of the mirror cell is defined on a grid with the step $\Delta x = \Delta y = \Delta z = 1$. Let us carry out similar calculations for the trajectories of individual particles $\tilde{\mathbf{x}}_e(t)$ and $\tilde{\mathbf{x}}_i(t)$ in the PIC model, neglecting the self-fields of these particles (particles do not create currents). Deviations of these trajectories $d\mathbf{x}_{e,i} = \mathbf{x}_{e,i}(t) - \tilde{\mathbf{x}}_{e,i}(t)$ from the trajectories of point particles in continuous fields are shown in Figs. 4c and 4d. It can be seen that during the simulation, the trajectory of the macro-proton deviates by a value less than the electron Larmor radius, and the deviation of the z-coordinate of the finite-size electron under the same conditions grows linearly with time (the faster, the larger the

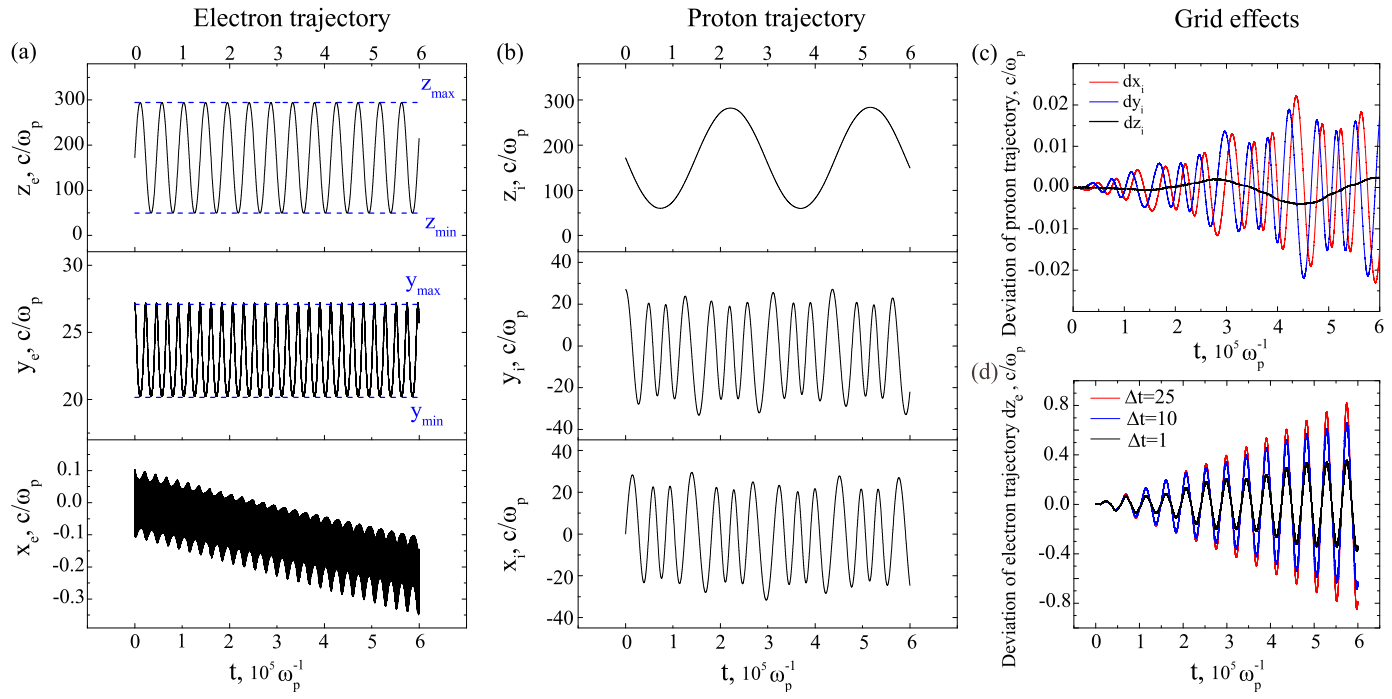

Fig. 4. The effect of a finite spatial grid on the trajectories of individual particles: (a) the trajectory of a test electron in the magnetic field of the mirror cell, (b) the trajectory of a proton in the magnetic field of the mirror cell, (c) the deviation of the trajectory of a point proton in a continuous magnetic field at $\Delta t = 25$ from trajectories of a macro-proton with a finite form-factor in a grid magnetic field, (d) a similar deviation of the z-coordinate of an electron at different time steps.

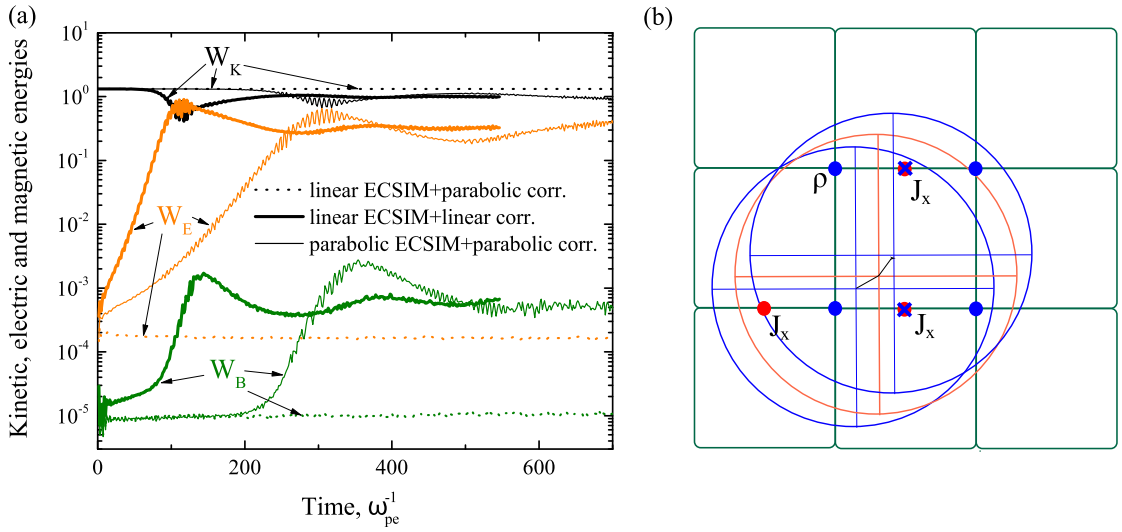

Fig. 5. (a) Evolution of the kinetic energy of all plasma particles W_K (black), the energy of the electric field W_E (orange) and the energy of the magnetic field W_B (green). Thick solid lines correspond to the case when the linear form-factor of particles (24) is used at both predictive and corrective steps, and thin solid lines — when both steps use the parabolic shape. The dotted lines show that the numerical instability disappears if the linear shape is used for the ECSIM predictive step, but the parabolic shape is used for corrective calculations of the Esirkepov currents. (b) Location of grid nodes where a particle with a linear form-factor gives a non-zero contribution over a time step (blue circles indicate nodes where the plasma density ρ changes, red circles indicate nodes for calculating the predicted current $\tilde{J}_x^{n+1/2}$ in the middle of the trajectory, blue crosses indicate nodes with the nonzero Esirkepov current $J_x^{n+1/2}$). (For interpretation of the colors in the figure(s), the reader is referred to the web version of this article.)

time step) and reaches the grid step. At the same time, at the stopping points, the dz_e deviation passes through zero; therefore, such an error does not lead to particle losses. However, it should be noted that the collisionless trajectory of particles should be accurately reproduced only at times between collisions. For a typical electron temperature of 50 eV, this time is $1.5 \cdot 10^5\ \omega_p^{-1}$. In this interval, the deviations turn out to be comparable with the electron gyro-radius, so the choice of the step $\Delta x = 1$ does not greatly impair the accuracy of the trajectory calculations which do not claim to resolve the Larmor rotation at large time steps.

3.3. Equilibrium homogeneous plasma

Let us now find out whether the proposed correction algorithm works correctly in the case of self-consistent dynamics of particles in the electromagnetic fields. For this purpose, it suffices to consider a homo-

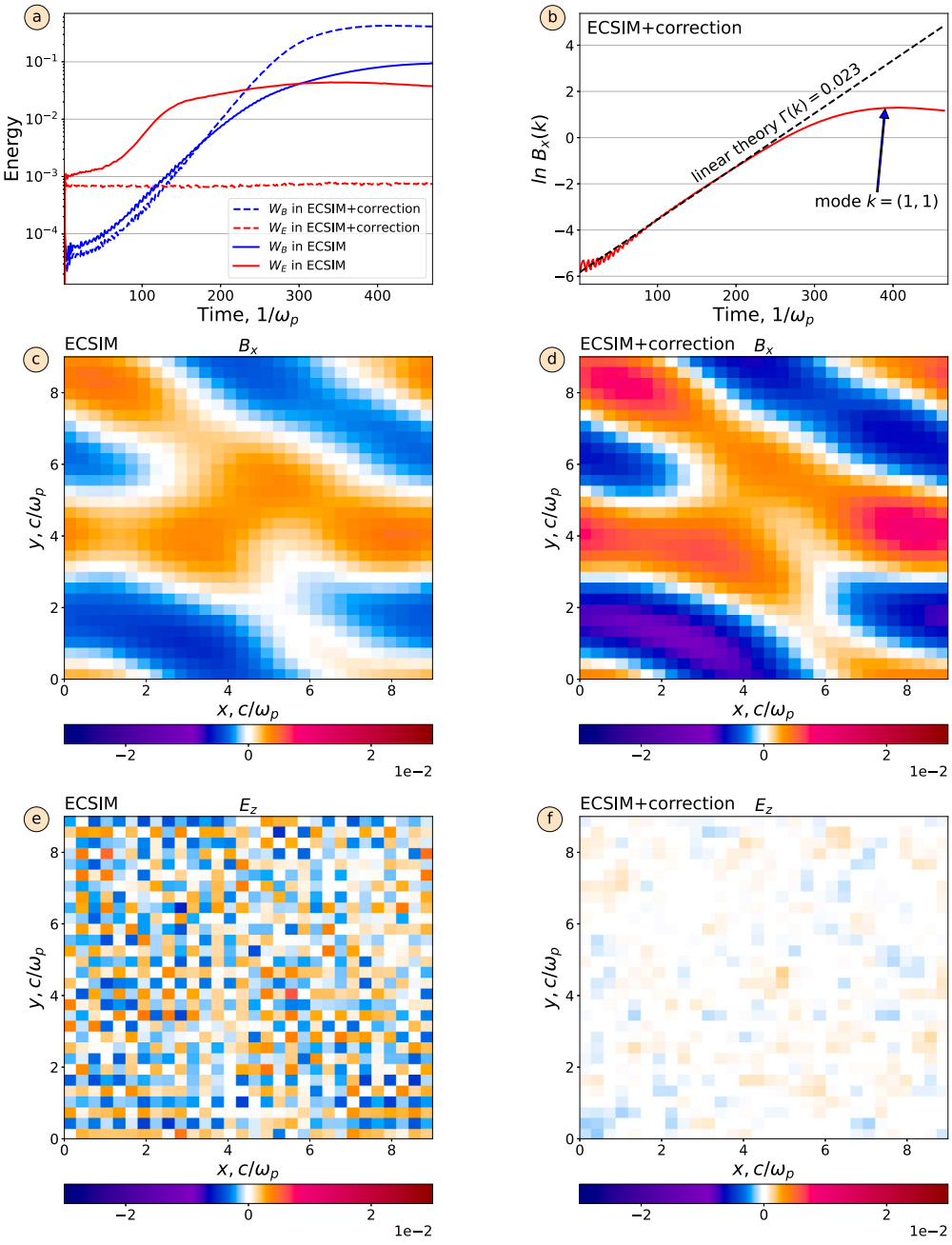

Fig. 6. Results of PIC simulations of the Weibel instability: (a) energies of the electric and magnetic fields in the ECSIM model with and without the correction step, (b) comparison of the theoretically predicted growth rate with the growth rate of the most unstable mode (1,1) of the B_x field actually observed in PIC simulations, (c) the map of the field $B_x(x, y)$ in the ECSIM model in the moment $\omega_p t = 255$, (d) similar $B_x(x, y)$ map in the ECSIM model with the correction step, (e) $E_z(x, y)$ field map in the ECSIM model at the same time, (f) similar $E_z(x, y)$ map in the ECSIM model with the correction step.

geneous isotropic unmagnetized plasma with the Maxwellian velocity distribution $f_e \propto \exp(-(v/v_T)^2/2)$ for electrons, assuming the ions to be a stationary compensating background. For the temperature $T = 100$ eV, the thermal velocity equals to $v_T = 0.014$. In this case, the grid step $\Delta x = 0.3$ exceeds the Debye radius by more than 20 times, and the time step $\Delta t = 1.5 = 5\Delta x$ significantly exceeds the CFL limit. Periodic conditions for particles and fields are used at the boundaries, which corresponds to the case of an infinite plasma.

If at the correction stage the Esirkepov current for individual particles is calculated using the same linear form-factor W (24) that was used at the prediction step, then the equilibrium plasma turns out to be unstable. As can be seen from Fig. 5a, where the history of the field and particle energies is shown by thick solid lines, the energy of the electric field W_E grows exponentially, taking energy away from the particles. Since the energy in this scheme is conserved exactly ($|W_K(t) - W_K(0) + W_E + W_B| < 10^{-13}$), the exponential growth saturates when half of the kinetic energy is converted into the field energy $W_E = W_K/2$. At a later stage, an increase in the magnetic field is also observed. The same instability, but with the reduced growth rate, develops if particles have a smoother parabolic shape at both steps (thin solid lines in Fig. 5a). The reason for the development of such a numerical instability is the strong local difference between the predicted and corrected currents. As is shown for the linear particle shape in Fig. 5b, the current calculated by the Esirkepov decomposition method (blue crosses) makes a non-zero contribution to fewer nodes than the current calculated from the particle shape $W(\mathbf{x}_p^{n+1/2} - \mathbf{x}_g)$ in the middle of its

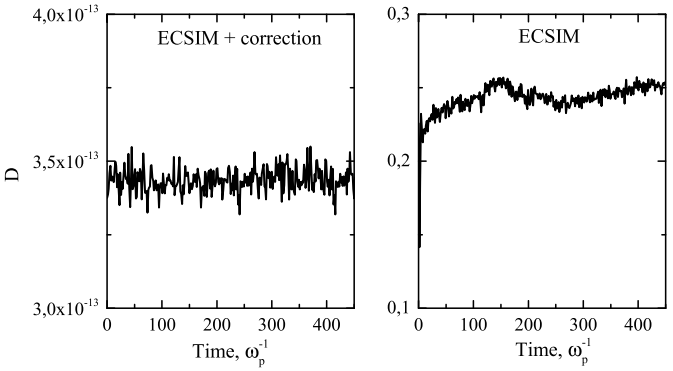

Fig. 7. Norm D as a function of time for the original ECSIM method and its corrected analog.

trajectory (red circles). A large local difference in currents requires a strong local correction of the fields, and hence the excitation of small-scale fluctuations. The need for precise conservation of energy requires fields to take energy from particles in response to an increase in the level of electromagnetic noise, which leads to the development of the instability.

To solve this problem, we propose to use different kernels for particles at the predictive and corrective steps. For example, if a particle has the linear shape at the ECSIM stage, it must have the parabolic shape at the stage of the Esirkepov current calculations. In this case, the Esirkepov current makes a non-zero contribution to the same nodes as the ECSIM current. The dotted lines in Fig. 5a show a stable level of thermal fluctuations if different form-factors are used at the predictive and corrective steps for the same macroparticles.

3.4. Weibel instability in a homogeneous anisotropic plasma

Let us check whether the proposed model accurately describes the known plasma instabilities that grow at low frequencies ($\omega \ll \omega_p$). As an example, we consider the aperiodic Weibel instability [32] developing in a uniform plasma with an anisotropic electron temperature ($T_\parallel > T_\perp$). In the absence of an external magnetic field, the dispersion relation for aperiodically growing perturbations with the frequency $\omega = i\Gamma$ and wavenumber $k = \sqrt{k_x^2 + k_y^2}$ in a plasma with the bi-Maxwellian distribution function $f_e \propto exp(-\beta_\perp(v_x^2 + v_y^2) - \beta_\parallel v_z^2)$ has the form [32]:

$$\Gamma^2 + k^2 - \frac{T_\parallel}{T_\perp} + 1 + \frac{T_\parallel}{T_\perp}\sqrt{\pi}\alpha e^{\alpha^2}\left(1 - \frac{2}{\sqrt{\pi}}\int_0^\alpha e^{-x^2}dx\right) = 0, \tag{25}$$

where $\beta_{\perp,\parallel} = m_e c^2/(2T_{\perp,\parallel})$, $\alpha = \Gamma\sqrt{\beta_\perp}/k$ and z is the parallel direction. The instability develops in a finite range of wavenumbers $k \in \left[0, \sqrt{T_\parallel/T_\perp - 1}\right]$. For the chosen parameters $T_\perp = 100$ eV, $T_\parallel = 1$ keV, the instability growth rate reaches its maximum value $\Gamma_{max} \approx 0.023\ \omega_p$ at $k \approx 1.14\ \omega_p/c$. Note that only magnetic field perturbations appear unstable in this problem.

Let us now study the development of the Weibel instability in the 3D PIC model, comparing the results obtained both in the framework of the original ECSIM method and in the case when this method is supplemented with a correction step that guarantees charge conservation. It can be seen from Fig. 6a that, if the Gauss law is not satisfied, the energy of the electrostatic noise increases along with the energy of the magnetic field. The influence of this noise turns out to be very significant, since it not only slows down the growth of energy in magnetic field perturbations at the linear stage, but also reduces the level of their nonlinear saturation. The dashed curves in Fig. 6a show that the inclusion of the correction step in the model stabilizes the electric field

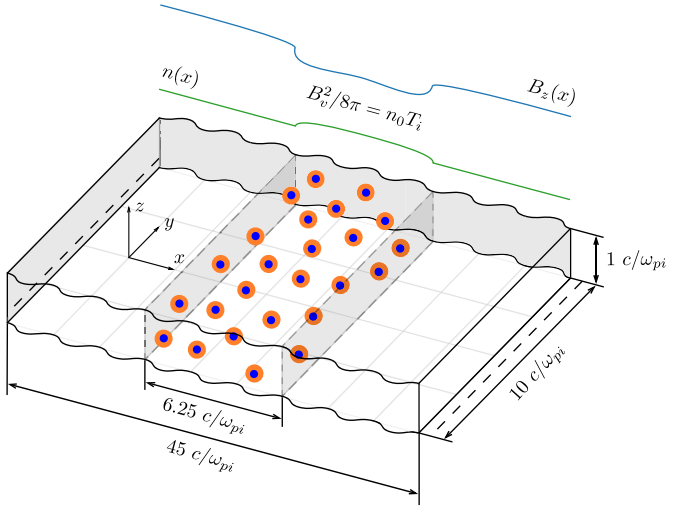

Fig. 8. Layout of the simulation domain in the problem of continuous plasma injection into a region with an initially uniform vacuum magnetic field.

energy at the level of the initial thermal noise, and also increases the magnetic field saturation energy by several times.

Since the computational domain in our PIC simulations is chosen to have sizes $L_x \times L_y \times L_z = 30\Delta x \times 30\Delta x \times 5\Delta x$ with the grid step $\Delta x = 0.3\ c/\omega_p$, among the possible set of discrete modes $k_{n,m} = \sqrt{n^2 + m^2}2\pi/L_x$, the highest growth rate should be achieved by the mode (1,1) with $k_{1,1} = 0.99$. Fig. 6b shows that the growth rate of this mode is in good agreement with the maximum theoretical growth rate calculated from the equation (25). Simulations in both models are carried out with the time step $\Delta t = 5\Delta x$, and the simultaneous charge and energy conservation is reached via the global correction of particle velocities (18). The effect of applying the corrective step is most clearly seen from the comparison between the electric field maps (Fig. 6e and 6f) obtained with and without fulfillment of the Gauss law. To illustrate how accurately the continuity equation can be satisfied after the correction step, we calculate the norm

$$D = \sqrt{\sum_g \left|\frac{\rho_g^{n+1} - \rho_g^n}{\Delta t} + (\mathrm{div}\,\mathbf{J}^{n+1/2})_g\right|^2}. \tag{26}$$

Comparison between the models based on the original ECSIM method and its corrected analog is shown in Fig. 7.

Lastly, we note that the corrective step has a little effect on the computation time which, in accordance with [31], is mainly spent on calculating the Lapenta matrix. Calculations on a single core of the Intel Xeon E5-2630v3 (2.4 GHz) processor show that the slowdown caused by the corrective step does not exceed 10%.

3.5. High-beta nonuniform plasma

To test high-β regimes, we consider the problem of plasma injection into the selected region of space with an initially uniform vacuum magnetic field $\mathbf{B} = (0, 0, B_v)$. This problem is closely related to the CAT experiment [10] where the high-pressure plasma in a compact mirror cell is created by the high-power neutral injection into a cold target plasma. Here, we will study this problem in the simplified formulation when the Maxwellian plasma is uniformly injected into a finite-width layer that is not limited in tangential directions. The same problem has been recently simulated using the explicit 2D3V PIC code [33] based on the standard Boris (leap-frog) and Yee (FDTD) algorithms. It has been found that, even if ions are much hotter than electrons, an electric current expelling the magnetic field from the injection region is created by the $\mathbf{E} \times \mathbf{B}$–drift of electrons rather than by the diamagnetic drift of

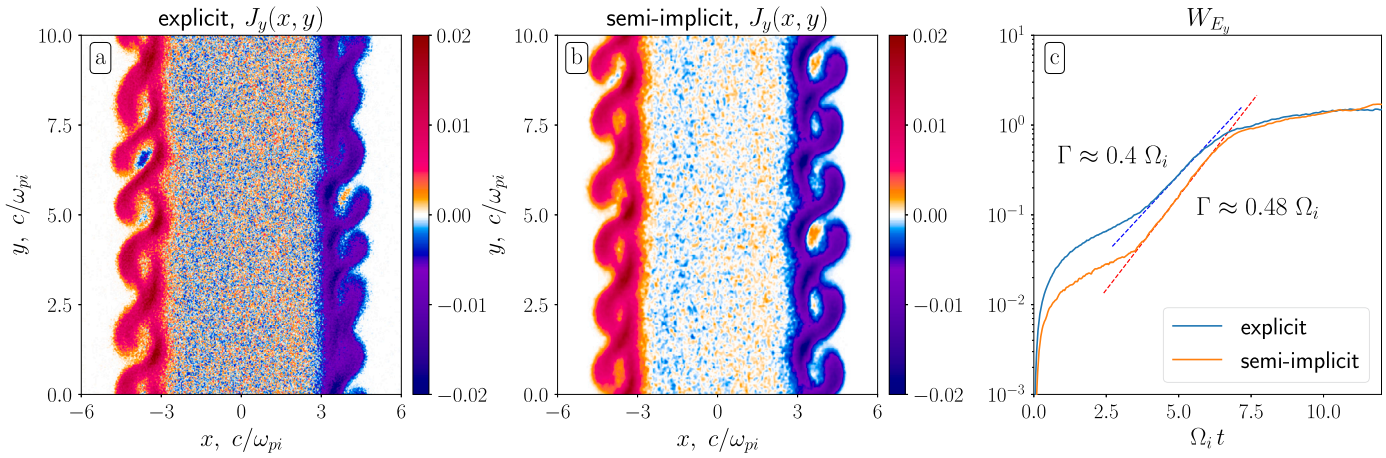

Fig. 9. Results of both explicit and semi-implicit PIC simulations for the drift ion-cyclotron instability in a high-β plasma: (a) the map of electric current density $J_y(x, y)$ measured in 2D explicit simulations [33] in the moment $t = 6.77/\Omega_i$, (b) the map of the z-averaged current $J_y(x, y)$ in the same moment of time in our semi-implicit 3D model (ECSIM+correction), (c) energy of E_y-field oscillations as a function of time (dashed lines describe the linear stage of the instability).

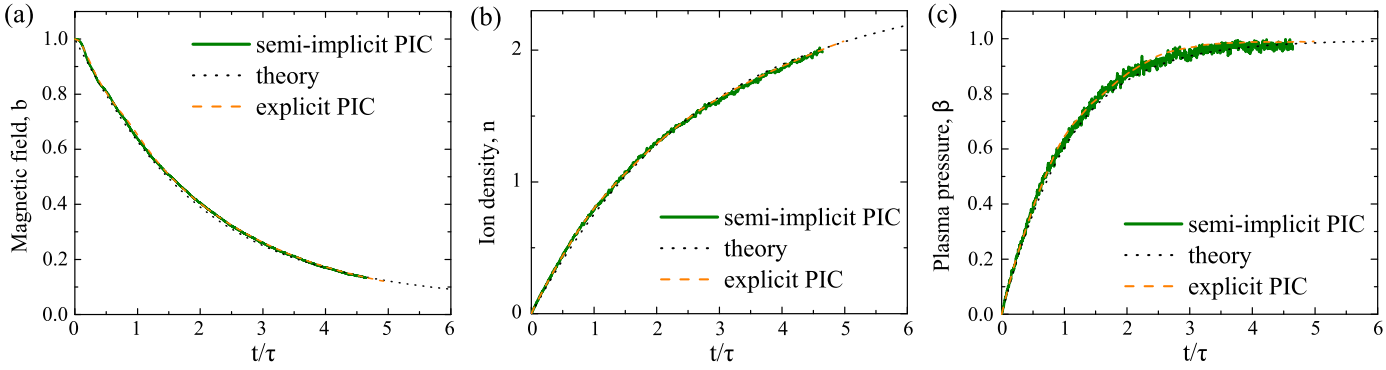

Fig. 10. Dynamics of the magnetic field, ion density and plasma pressure in the center of the injection region.

ions. This current layer has been also shown to be unstable against perturbations at the ion-cyclotron frequency harmonics traveling with the electron drift velocity. In addition, the deepening of the magnetic well with the growth of plasma pressure has been found to be well described by a simple theory. The conclusion about instability of high-β plasma boundaries is very important for the confinement of hot ions in mirror traps, that is why we should check if the same instability is reproduced in our semi-implicit PIC model. Our simulations should also reproduce the same law of magnetic field exclusion from the injection region.

To compare with the results obtained in the paper [33], we simulate the problem using the proposed semi-implicit PIC model for the same physical parameters. Electron-ion pairs with temperatures $T_i = 10$ keV, $T_e = 2$ keV and mass ratio $m_i/m_e = 16$ are uniformly thrown into the injection region occupying the central part of the computational domain (Fig. 8) so that, by the time $\tau = 1000\ \omega_{pe}^{-1}$, the linearly growing plasma density should reach the value of $n_0 = 10^{13}$ cm^{-3} we choose as unity. The initially uniform vacuum magnetic field equals to $B_v = \sqrt{2T_i/(m_e c^2)} \approx 0.1978$, therefore, by the time $t \simeq \tau$, the plasma pressure should become close to the magnetic field pressure ($\beta \simeq 1$). To compare with 2D simulations, we minimize 3D effects by reducing the size of the computational domain along the vacuum magnetic field to the minimal value $L_z = 5\Delta z$. The time and space steps are chosen to be much greater than in the explicit PIC model ($\Delta t = 0.5$ and $\Delta x = \Delta y = \Delta z = 0.2$ instead of $\Delta t = 0.025$ and $\Delta x = \Delta y = 0.05$ in [33]). The acceptable level of noise is achieved by using 200 computational particles per cell at the unit density. We use periodic boundary conditions along the y and z directions, and absorbing conditions for both fields and particles in the x direction.

Let us first make sure that the ion-cyclotron instability observed in the paper [33] is also developed at the boundaries of our injection region. Fig. 9 shows the spatial distributions of electric current J_y measured in the moment $t = 6.77/\Omega_i = 0.548\ \tau$ in both explicit and semi-implicit PIC models. One can see that the current layers are unstable against flute-like perturbations with the same wavenumbers. The stage of exponential growth of this instability is clearly seen in Fig. 9c where the energy of electric field E_y associated with the unstable perturbations is shown as a function of time. The growth rate in different models is found to be close to $\Omega_i/2$, although it seems to be slightly underestimated in the explicit model (blue curve) because of a higher level of noise.

According to the theory proposed in [33], the deepening of the magnetic well produced by the plasma in the center of the injection region slows down as the plasma pressure approaches the limit of $\beta \approx 1$. This theory can be reformulated in a more simple way if the vacuum magnetic field is chosen slightly higher ($B_v = \sqrt{2(T_i + T_e)/(m_e c^2)}$ instead of $B_v = \sqrt{2T_i/(m_e c^2)}$):

$$\frac{t}{\tau} = \frac{1-b^2}{4} - \ln b^{3/2} + \frac{\sqrt{\pi}}{8l}(1-b)\left(1+\frac{3}{b}\right), \tag{27}$$

$$n(t) = \frac{\sqrt{b}}{3}\left(1-b^{3/2}\right) + 3\left(1-\sqrt{b}\right), \tag{28}$$

$$\beta(t) = 1 - b^2, \tag{29}$$

where $b(t) = B(t,0)/B_v$ is the magnetic field at the center of the injection region, $n(t)$ is the ion density, and $\beta(t)$ is the plasma pressure in units of the vacuum magnetic field pressure $B_v^2/2$, $l = 3.125\ c/\omega_{pi}$ is the half-width of the injection region. Fig. 10 shows good agreement

of the simulation results obtained in both explicit and semi-implicit PIC models for the new vacuum field value $B_v \approx 0.2167$ with the theoretical predictions.

4. Conclusion

To simulate high-beta regimes of plasma confinement in mirror traps, we propose a new PIC model based on the semi-implicit ECSIM method combined with the correction step allowing to satisfy both the energy and charge conservation laws. The implicit nature of the scheme makes it possible not to resolve the plasma frequency and the Debye radius, and for relatively large steps $\Omega_e \Delta t \ll B/(|\nabla B|\rho_e)$ the model allows one to reproduce the electron dynamics in the drift approximation. For simultaneous conservation of both energy and charge, the proposed PIC model uses a two-stage predictor-corrector scheme, where, by analogy with the work of [27], the predictive stage is based on the energy-saving ECSIM method, and the corrective stage provides a transition to a charge-saving current. In our work, this approach was implemented for the standard Yee mesh and required a significant modification of the correction step. The final current is calculated in our model using the Esirkepov density decomposition method, and not only the electric but also the magnetic field is corrected. In this case, the law of energy conservation is achieved by renormalizing the particle velocities in accordance with the work done on them by the electric field. Due to the possibility of separating the contributions of individual particles in the Esirkepov current, such a renormalization can be not only local (with its own coefficient for each cell), but also individual for each kind of particles. An important feature of the proposed correction method is the need to use different form factors for the same particle at the predictive and corrective steps. The new PIC model is shown to reproduce not only the well-known Weibel instability of a homogeneous unmagnetized plasma with temperature anisotropy, but also the drift ion-cyclotron instability growing at the boundary of a high-β plasma during plasma injection into the vacuum magnetic field. The model also correctly describes the deepening of the magnetic well in time under this continuous plasma injection.

CRediT authorship contribution statement

E.A. Berendeev: Investigation, Software, Validation, Visualization. **I.V. Timofeev:** Conceptualization, Investigation, Supervision, Validation, Writing – original draft. **V.A. Kurshakov:** Investigation, Validation.

Declaration of competing interest

The authors declare that they have no known competing financial interests or personal relationships that could have appeared to influence the work reported in this paper.

Data availability

Data will be made available on request.

References

[1] A.D. Beklemishev, Diamagnetic 'bubble' equilibria in linear traps, Phys. Plasmas 23 (2016) 082506.

[2] M.S. Khristo, A.D. Beklemishev, High-pressure limit of equilibrium in axisymmetric open traps, Plasma Fusion Res. 14 (2019) 2403007.

[3] M.S. Khristo, A.D. Beklemishev, Two-dimensional MHD equilibria of diamagnetic bubble in gas-dynamic trap, Plasma Phys. Control. Fusion 64 (2022) 095019.

[4] J. Park, N.A. Krall, P.E. Sieck, D.T. Offermann, M. Skillicorn, A. Sanchez, K. Davis, E. Alderson, G. Lapenta, High-energy electron confinement in a magnetic cusp configuration, Phys. Rev. X 5 (2015) 021024.

[5] J. Park, G. Lapenta, D. Gonzalez-Herrero, N.A. Krall, Discovery of an electron gyroradius scale current layer: its relevance to magnetic fusion energy, Earth's magnetosphere, and sunspots, Front. Astron. Space Sci. 6 (74) (2019).

[6] H. Gota, M.W. Binderbauer, T. Tajima, S. Putvinski, M. Tuszewski, B.H. Deng, S.A. Dettrick, D.K. Gupta, S. Korepanov, R.M. Magee, et al., Formation of hot, stable, long-lived field-reversed configuration plasmas on the C-2W device, Nucl. Fusion 59 (2019) 112009.

[7] S.A. Dettrick, D.C. Barnes, F. Ceccherini, L. Galeotti, S.A. Galkin, S. Gupta, K. Hubbard, O. Koshkarov, C.K. Lau, Y. Mok, et al., Simulation of equilibrium and transport in advanced FRCS, Nucl. Fusion 61 (2021) 106038.

[8] Yue Peng, Yong Yang, Yuesong Jia, Bo Rao, Ming Zhang, Zhijiang Wang, Hongyu Wang, Yuan Pan, Simulation on formation process of field-reversed configuration, Nucl. Fusion 62 (2022) 066037.

[9] Yu.A. Tsidulko, I.S. Chernoshtanov, Particle-in-cell simulation of field reversal in mirror trap with neutral beam injection, AIP Conf. Proc. 1771 (2016) 040005; https://doi.org/10.1063/1.4964190.

[10] P.A. Bagryansky, T.D. Akhmetov, I.S. Chernoshtanov, P.P. Deichuli, A.A. Ivanov, A.A. Lizunov, V.V. Maximov, V.V. Mishagin, S.V. Murakhtin, E.I. Pinzhenin, et al., Status of the experiment on magnetic field reversal at BINP, AIP Conf. Proc. 1771 (2016) 030015.

[11] J.P. Boris, Relativistic plasma simulation-optimization of a hybrid code, in: Proc. of 4th Conf. on Numerical Simulations of Plasmas, Washington, DC, USA 2–3 November 1970, Naval Research Laboratory, Washington, DC, USA, 1970, pp. 3–67, https://books.google.ru/books?id=zqxSAQAACAAJ.

[12] K. Yee, Numerical solution of initial boundary value problems involving Maxwell's equations in isotropic media, IEEE Trans. Antennas Propag. 14 (3) (1966) 302–307, https://doi.org/10.1109/TAP.1966.1138693.

[13] M.A. Boronina, G.I. Dudnikova, A.A. Efimova, E.A. Genrikh, V.A. Vshivkov, I.S. Chernoshtanov, Numerical study of diamagnetic regime in open magnetic trap, Inst. Phys. Conf. Ser. 1640 (2020) 012021, https://doi.org/10.1088/1742-6596/1640/1/012021.

[14] Atul Kumar, Juan F. Caneses Marin, Kinetic simulations of collision-less plasmas in open magnetic geometries, Plasma Phys. Control. Fusion 64 (2022) 035012.

[15] D.P. Fulton, C.K. Lau, I. Holod, Z. Lin, S. Dettrick, Gyrokinetic particle simulation of a field reversed configuration, Phys. Plasmas 23 (2016) 012509, https://doi.org/10.1063/1.4930289.

[16] S. Markidis, G. Lapenta, The energy conserving particle-in-cell method, J. Comput. Phys. 230 (2011) 7037–7052, https://doi.org/10.1016/j.jcp.2011.05.033.

[17] L.F. Ricketson, L. Chacón, An energy-conserving and asymptotic-preserving charged-particle orbit implicit time integrator for arbitrary electromagnetic fields, J. Comput. Phys. 418 (2020) 109639, https://doi.org/10.1016/j.jcp.2020.109639.

[18] A.B. Langdon, B.I. Cohen, A. Friedman, Direct implicit large time-step particle simulation of plasmas, J. Comput. Phys. 51 (1983) 107–138.

[19] D.R. Welch, D.V. Rose, R.E. Clark, T.C. Genoni, T. Hughes, Implementation of an non-iterative implicit electromagnetic field solver for dense plasma simulation, Comput. Phys. Commun. 164 (1) (2004) 183–188.

[20] J. Brackbill, D. Forslund, An implicit method for electromagnetic plasma simulation in two dimensions, J. Comput. Phys. 46 (1982) 271, https://doi.org/10.1016/0021-9991(82)90016-X.

[21] K. Noguchi, C. Tronci, G. Zuccaro, G. Lapenta, Formulation of the relativistic moment implicit particle-in-cell method, Phys. Plasmas 14 (2007) 042308, https://doi.org/10.1063/1.2721083.

[22] A. Kempf, P. Kilian, U. Ganse, C. Schreiner, F. Spanier PICPANTHER, A simple, concise implementation of the relativistic moment implicit particle-in-cell method, Comput. Phys. Commun. 188 (2015) 198–207, https://doi.org/10.1016/j.cpc.2014.11.010.

[23] G. Lapenta, Exactly energy conserving semi-implicit particle in cell formulation, J. Comput. Phys. 334 (2017) 349–366.

[24] J.R. Angus, A. Link, A. Friedman, D. Ghosh, J.D. Johnson, On numerical energy conservation for an implicit particle-in-cell method coupled with a binary Monte-Carlo algorithm for Coulomb collisions, J. Comput. Phys. 456 (2022) 111030.

[25] T.Zh. Esirkepov, Exact charge conservation scheme for Particle-in-Cell simulation with an arbitrary form-factor, Comput. Phys. Commun. 135 (2001) 144–153.

[26] Y. Chen, G. Tóth, Gauss's law satisfying energy-conserving semi-implicit particle-in-cell method, J. Comput. Phys. 386 (2019) 632–652.

[27] M. Campos Pinto, V. Pagès, A semi-implicit electromagnetic FEM-PIC scheme with exact energy and charge conservation, J. Comput. Phys. 453 (2022) 110912, https://doi.org/10.1016/j.jcp.2021.110912.

[28] I. Kotelnikov, On the structure of the boundary layer in a Beklemishev diamagnetic bubble, Plasma Phys. Control. Fusion 62 (2020) 075002, https://doi.org/10.1088/1361-6587/ab8a63.

[29] S.E. Parker, C.K. Birdsall, Numerical error in electron orbits with large $\omega_{ce}\Delta t$, J. Comput. Phys. 97 (91) (1991).

[30] H.X. Vu, J.U. Brackbill, Accurate numerical solution of charged particle motion in a magnetic field, J. Comput. Phys. 116 (2) (1995) 384.

[31] D. Gonzalez-Herrero, E. Boella, G. Lapenta, Performance analysis and implementation details of the Energy Conserving Semi-Implicit Method code (ECsim), Comput. Phys. Commun. 229 (2018) 162.

[32] E.S. Weibel, Spontaneously growing transverse waves in a plasma due to an anisotropic velocity distribution, Phys. Rev. Lett. 2 (3) (1959) 83.

[33] V.A. Kurshakov, I.V. Timofeev, The role of electron current in high-β plasma equilibria, Phys. Plasmas 30 (2023) 092513.